# Non Inductive Current Drive and Beam Plasma Interaction in Compact Tori

R. Farengo 1), A. Lifschitz 2), K. Caputti 1), N. Arista 1) and R. A. Clemente 3)

1) Centro Atómico Bariloche e Instituto Balseiro, Bariloche, RN, Argentina.
2) Consejo Nacional de Investigaciones Científicas y Técnicas, Argentina
3) Universidade Estadual de Campinas, Campinas, SP, Brasil

e-mail contact of main author: farengo@cab.cnea.gov.ar

**Abstract**. The effect of a steady toroidal field (TF) on rotating magnetic field (RMF) current drive, the interaction of neutral beams with Field Reversed Configurations (FRC) and the *relaxed* (minimum dissipation) states of tokamaks sustained by helicity injection are studied.

## 1. Effect of a Steady Toroidal Field on RFM Current Drive

RMFs have been used to drive current in Rotamaks, FRCs and spherical tokamaks (ST) [1]. We consider an infinitely long, hollow, plasma column with a finite radius conductor running along its axis. The physical model is the same as in most previous studies, fixed ions and Ohm's law with the Hall term for electrons. Instead of using a Fourier decomposition in θ a fully 2D ($r$, θ) numerical code that solves the time dependent problem is employed.

The coils that produce the RMF are assumed to be far from the plasma and the RMF is written as: $B_r^{rot} = B_\omega \cos(\omega t - \theta)$, $B_\theta^{rot} = B_\omega \sin(\omega t - \theta)$. Using Ohm's law and Maxwell's equations a set of equations for $B_z$ and $A_z$ can be obtained. $A_z$ is separated in two parts: $A_z = A_{z,vac} + A_{z,pl}$, where $A_{z,vac}$ contains the contribution of the stationary axial current (calculated analytically) and $A_{z,pl}$ the contribution of the plasma and the external coils. Normalizing the radius with $r_b$ (outer plasma radius) the following dimensionless equations are obtained:

$$\frac{\partial A}{\partial \tau} = \frac{1}{2\lambda^2}\left\{\nabla^2 A + \frac{\gamma}{r}\left[\left(\frac{\partial A}{\partial r} - \frac{B_{tor}}{r}\right)\frac{\partial B}{\partial \theta} - \frac{\partial A}{\partial \theta}\frac{\partial B}{\partial r}\right]\right\}$$

$$\frac{\partial B}{\partial \tau} = \frac{1}{2\lambda^2}\left\{\nabla^2 B + \frac{\gamma}{r}\left[\frac{\partial}{\partial r}\left(\nabla^2 A\right)\frac{\partial A}{\partial \theta} - \frac{\partial}{\partial \theta}\left(\nabla^2 A\right)\left(\frac{\partial A}{\partial r} - \frac{B_{tor}}{r}\right)\right]\right\} \qquad (1)$$

where:

$$B = \frac{B_z}{B_\omega}, \qquad A = \frac{A_{z,pl}}{B_\omega r_b}, \qquad \tau = \omega t, \quad \lambda = r_b\left(\frac{\mu_0 \omega}{2\eta}\right)^{1/2}, \qquad \gamma = \frac{B_\omega}{en\eta},$$

η is the resistivity, assumed uniform, and $B_{tor}$ is the vacuum toroidal field at $r$=1, normalized to $B_\omega$. Knowing $A$ and $B$, the other magnetic field components can be easily calculated. To solve Eqs. (1) we need boundary conditions at the inner ($r=r_a$) and outer plasma boundaries. $A$ must provide the desired RMF far enough from the plasma and have a continuous radial derivative ($B_\theta = -\partial A_z/\partial r$) at both boundaries. $B$ is uniform both inside and outside the plasma column but its value on the inside changes with time due to changes in the plasma current.

The efficiency is defined as the ratio between the azimuthal plasma current and the current that would be produced if all the electrons rotate rigidly with frequency ω. Fig. 1 is a plot of

the steady-state efficiency vs. $B_{tor}$ for $\gamma$ =14.9, $\lambda$=11.07 and $r_a$=0.15. The aspect ratio is $A_r=(r_b+r_a)/(r_b-r_a)$=1.35. In an FRC, these values of $\lambda$ and $\gamma$ result in incomplete field penetration and an efficiency of 0.42 [2]. For small values of $B_{tor}$ ($B_{tor}< B_{tor}^{crit}\cong$1.26) there are two solutions. The initial conditions determine the branch towards which the system evolves. If we set $B_{tor}< B_{tor}^{crit}$ and start with a plasma that has no azimuthal current, the solution follows the low efficiency branch (LEB) (dashed line) in Fig. 1. When $B_{tor}$ becomes larger than the critical value, and the same initial conditions are used, the efficiency *jumps* to the high efficiency branch (HEB) (full line). To access the HEB for $B_{tor}$ less than the critical value (dotted line) it is necessary to start with a solution having $B_{tor} > B_{tor}^{crit}$ and slowly decrease $B_{tor}$. In the HEB the efficiency decreases with $B_{tor}$ while in the LEB the efficiency initially increases and later decreases. This behavior was observed in the experiments [1] and also reported in Ref. [3]. With the same value of $\lambda$, and $\gamma$ =16.6, the efficiency obtained for an FRC is unity. Using these values $\lambda$ and $\gamma$, and $B_{tor}$ =0, we also obtained an efficiency of 1. As $B_{tor}$ increases, the efficiency decreases taking similar values to those shown in the HEB of Fig. 1. For $0.53\leq B_{tor}\leq 0.77$ there is another solution.

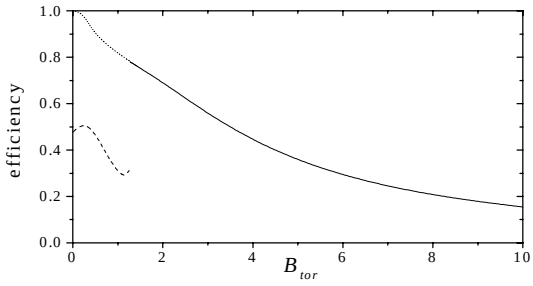


*FIG. 1. Efficiency vs. steady TF for $\gamma$=14.9, $\lambda$=11.07 and $r_a$=0.15.*

The effect of the steady TF on the azimuthal current density profile is shown in Figs. 2 and 3, which present plots of the averaged (over $\theta$) $j_\theta$ vs. $r$ for the two branches shown in Fig. 1. Fig. 2 corresponds to the LEB and Fig. 3 to the HEB; three values of $B_{tor}$ are considered in both cases. In Fig. 2, when $B_{tor}$ =0 (full line) there is a large region, up to $r\cong$0.5, inside the plasma with negligible $j_\theta$ and a narrow region, $r\geq$0.9, on the outside where the electrons rotate rigidly with frequency $\omega$. When $B_{tor}$=0.5 (dashed line) $j_\theta$ increases on the inside, in the region $0.3\leq r\leq$ 0.5, and decreases for $r\geq$0.6, giving an overall increase in the total plasma current. Finally, when $B_{tor}$=1.15, $j_\theta$ is comparable to that obtained with $B_{tor}$=0 for $r\leq$0.6 and significantly smaller at larger radius. In Fig. 3, when $B_{tor}$=0 the efficiency is 1 and the electrons rotate with frequency $\omega$ everywhere. As the steady TF increases ($B_{tor}$=4, dashed line), a region with negligible, even reversed, current density appears. As $B_{tor}$ increases further ($B_{tor}$=8.0, dotted line) the width of this region increases.

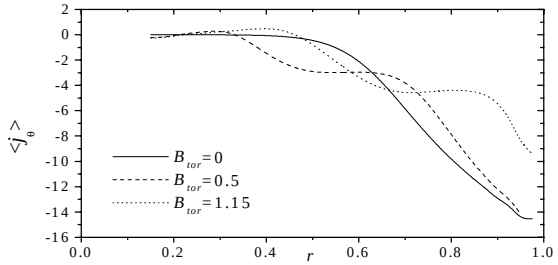


*FIG. 2. Averaged $j_\theta$ vs. r for LEB*

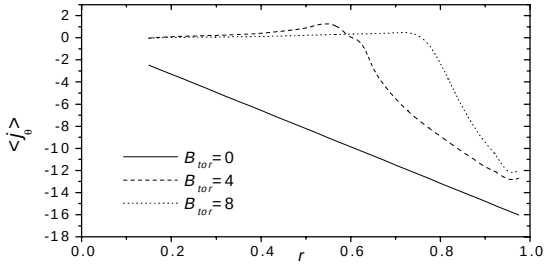


*FIG. 3. Averaged $j_\theta$ vs. r for HEB.*

The existence of diamagnetic poloidal currents was studied for the two branches considered above. For the LEB there is a significant diamagnetic effect, with a reduction of more than 20% in the total azimuthal field (compared to the vacuum field) when $B_{tor}$=1.15. For the HEB the diamagnetism is negligible (less than 3%).

## 2. Beam-plasma interaction in FRCs

Neutral beam injection is one of the methods proposed for heating and current drive in FRCs. In addition, it can supply a population of large gyroradius ions which contribute to stabilizing the internal tilt mode. Experiments on neutral beam injection have begun recently [4]. We study the interaction of a neutral beam with an FRC plasma. This includes the ionization of the neutral atoms and the transference of momentum and energy to the plasma. The current carried by the beam and the changes it produces in the equilibrium are also calculated. The Monte-Carlo code employed follows the actual trajectories (no gyro-averaging) of an ensemble of particles. This is necessary in FRCs because the lack of toroidal field results in complex orbits, with large radial excursions, for the energetic particles.

The ionization processes included are ionization by collisions with electrons and ions and by charge exchange; both from the ground and from excited states. The effect of Coulomb collisions is introduced via Fokker-Planck operators which are used to calculate the power and momentum transferred to electrons and ions. An iterative algorithm is used to calculate the self-consistent beam current and the 3D density and magnetic field profiles. Starting with a given equilibrium the beam code is employed to calculate the stationary beam current produced by continuous injection. A Grad-Shafranov equation that includes a term with the beam current is then solved to calculate a new equilibrium and the sequence (beam code plus equilibrium code) is repeated until the solutions converge. In the Grad-Shafranov equation, the relationship between the pressure *(P)* and the magnetic flux is assumed to be: $P=G_0[\psi/\psi_0-D(\psi/\psi_0)^2]$, where $G_0$ is a constant, $\psi_0$ is the flux at the magnetic null and $D$ is a parameter that controls the shape of the equilibrium. The equilibria have elliptical shape, with peaked current profile, for $D<0$, and racetrack shape, with hollow profile, for $D>0$. The equilibria considered have a cylindrical separatrix with a radius of 30 cm and a half length of 120 cm. The external magnetic field is 5 kG, the temperature is 800 eV and the radius of the magnetic null is 21 cm. The peak density results 8-10x$10^{14}$ $cm^{-3}$.

The injection geometry is shown in Fig. 4. We consider a mono-energetic deuterium beam injected in a deuterium plasma and restrict to midplane ($z$=0) injection perpendicular to the FRC axis. The impact parameter ($b$) is important in determining the initial value of the azimuthal component of the velocity ($v_\theta$) of the ions (just after ionization). Particles injected with small $b$ are ionized with low $v_\theta$, and follow orbits with large radial excursions. On the other hand, particles injected with $b$ around or above the null radius are trapped in orbits with larger $v_\theta$. In spite of these differences, the total azimuthal current carried by the trapped beam ($I_b$) does not change very much. The particles with large radial oscillations (small $b$) carry less current, but spend more time in low density regions. Therefore, they take longer to slow down and compensate their lower current (smaller $v_\theta$) with their longer slow down times.

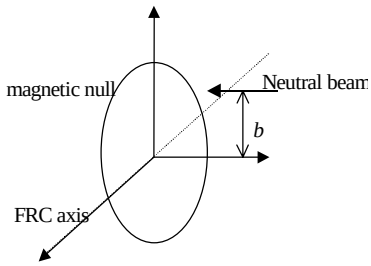

*FIG. 4 Injection geometry*

The dependence of the beam current ($I_b$) with the neutral injection current ($I_N$) and the energy of the neutral atoms ($E_N$) is shown in Figs. 5 and 6 respectively. In Fig. 5, the relationship deviates from linear because the beam modifies the magnetic field, increasing the density around the injection region. In the peaked case this occurs at lower beam currents and the region of linear behavior is smaller. For high $I_N$ and $E_N$ (Fig. 6) the beam current is larger in

the hollow case than in the peaked case. This is due to the larger density increase produced by the beam in the second case.

Figs. 7 and 8 show the power transferred to the electrons ($P_e$), to the ions ($P_i$) and the total value ($P_t$) as a function of $E_N$, for hollow and peaked plasmas respectively. For low $E_N$, the beam particles transfer most of the power to the ions. When $E_N$ increases, and the velocity of the beam particles approaches the mean electron velocity, most of the power is transferred to the electrons. The difference between the transferred power and the injected one ($P_N$) is due to particle losses. The losses occur mostly at the ends of the FRC, and are larger in hollow than in peaked equilibria. For higher $E_N$, the self-confining effect reduces the beam spread and therefore the losses at the ends, improving the efficiency of the power transfer.

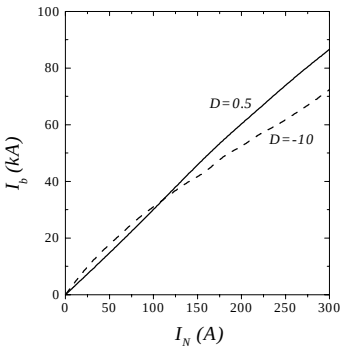


*FIG 5: beam current vs. injected current of neutral atoms. $E_N$=20 keV.*

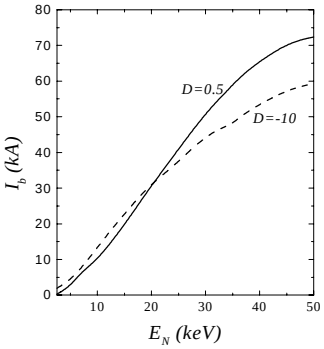


*FIG 6: beam current vs. energy of neutral atoms. $I_N$=100 A.*

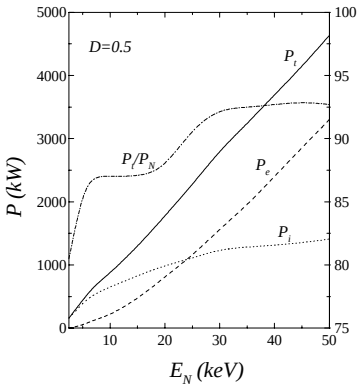


*FIG 7: Transferred power vs. neutral atoms energy. $I_N$=100 A.*

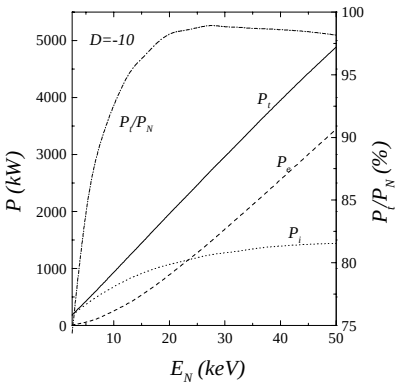


*FIG 8: Transferred power vs. neutral atoms energy. $I_N$=100 A.*

## 3. Minimum dissipation states in tokamaks sustained by coaxial helicity injection

In driven systems, the minimum dissipation principle could be more appropriate than the minimum energy principle because it allows for the introduction of balance constraints (injection=dissipation) and non uniform/anisotropic resistivity effects. We used the principle of minimum rate of energy dissipation to calculate relaxed states for tokamaks with anisotropic resistivity sustained by coaxial helicity injection. To minimize the Ohmic dissipation rate with the constraints of helicity balance (injection rate=dissipation rate) and $\nabla\cdot\mathbf{B}$=0 the following functional was introduced:

$$W = \int \left(\eta_{//}\, \boldsymbol{j}_{//}^2 + \eta_{\perp}^2 \boldsymbol{j}_{\perp}^2\right) d\tau - \frac{\lambda}{\mu_0}\left(\int \eta_{//}\left(\mathbf{j}\cdot\mathbf{B}\right)\, d\tau + \oint \varphi\ \mathbf{B}\cdot\mathbf{dS}\right) - \int \gamma\ \nabla\cdot\mathbf{B}\ d\tau$$

where // and $\perp$ refer to the direction of the magnetic field, $\eta$ is the resistivity, $\varphi$ is the applied electrostatic potential and $\lambda$ and $\gamma$ are Lagrange multipliers. The Euler-Lagrange equations obtained by setting the first variation of *W* ($\delta W$) equal to zero were solved numerically (in 2D) using boundary conditions that include the basic features of the experimental situation (existence of *magnetized* electrodes for helicity injection) and result in the cancellation of the surface term in $\delta W$.

The configuration considered is basically the same employed in Ref. [5] and is shown in Fig. 9 . The tokamak chamber is formed by two electrodes separated by insulators and a coil provides the magnetic field needed for helicity injection. The axial current ($I_{TF}$) produces the vacuum toroidal field. Figs. 10, 11 and 12 present plots of the midplane ($z$=0) toroidal current density ($j_\theta$), toroidal magnetic field ($B_\theta$) and ratio of these two quantities ($\mu_0 j_\theta/B_\theta$) as a function of radius for three values of $c$. This parameter is the ratio between the parallel and perpendicular resistivities ($c=\eta_{//}/\eta_\perp$) and it is changed by increasing $\eta_\perp$ while $\eta_{//}$ remains fixed. Fig. 11 shows that $B_\theta$ remains almost unchanged for the three values of $c$ and decays (with $r$) almost as a vacuum field. The toroidal current density (Fig. 10) decreases as $c$ is reduced but the shape of the profile remains basically the same. The ratio $\mu_0 j_\theta/B_\theta$ is a very important quantity in relaxation theory and its shape changes significantly when $c$ is reduced. The results obtained for $c$=1 (isotropic resistivity) do not agree with those of Ref. [5] which, unfortunately, are not correct.

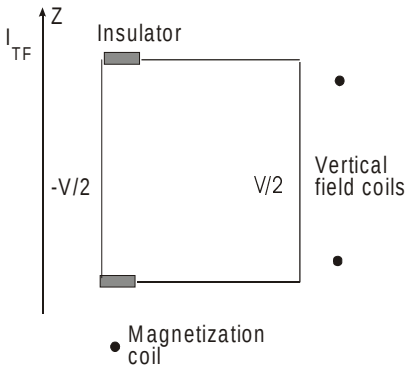


*FIG.9, Configuration considered*

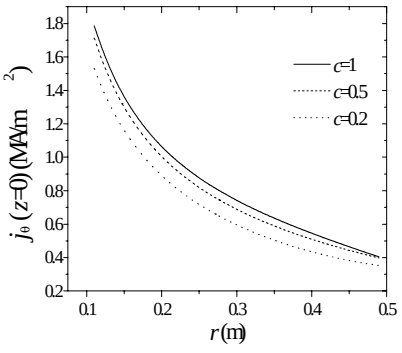


*FIG. 10. $j_\theta(z=0)$vs. r*

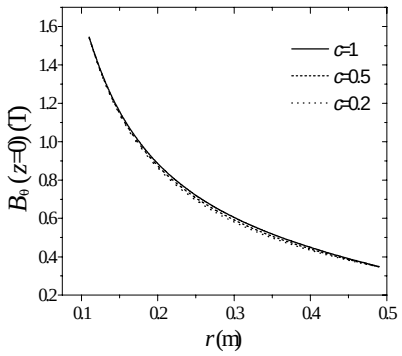


*FIG. 11. $B_\theta(z=0)$vs. r*

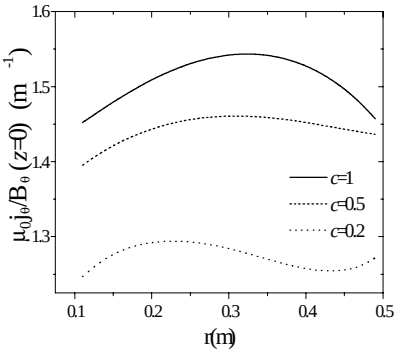


*FIG. 12 $\mu_0 j_\theta/B_\theta$ (z=0) vs. r*


## Acknowledgements

This work was partially supported by IAEA contract Nº 10527/RI.


## References


[1] JONES I. R., "A review of rotating magnetic field current drive and the operation of the rotamak as a field-reversed configuration (Rotamak-FRC) and a spherical tokamak (rotamak-ST)". Phys. Plasmas **6**, 1950 (1998).
[2] MILROY, R. D., "A numerical study of rotating magnetic fields as a current drive for field reversed configurations". Phys. of Plasmas **7**, 111 (1999).
[3] BERTRAM,W. K.,"The effect of a steady azimuthal field on rotating magnetic field current drive" J. Plasma Phys. **37**, 423 (1987).
[4] ASAI, T. et al. "Experimental evidence of improved confinement in a high-beta field - reversed configuration plasma by neutral beam injection". Phys. of Plasmas **7**, 2294 (2000).
[5] ZHANG C. et al. "Relaxed state for the coaxial helicity injection current drive in toroidal plasmas", Phys. Plasmas **5**, 178 (1998).